Improved CASA model based on satellite remote sensing data: Simulating net primary productivity of Qinghai Lake Basin alpine grassland

Chengyong Wu[1,3], Kelong Chen[2,3], Chongyi E[2,3], Xiaoni You[1], Dongcai He[1], Liangbai Hu[1], Baokang Liu[1], Runke Wang[1], Yaya Shi[1],Chengxiu Li[1], and Fumei Liu[2]

[1]School of Resources and Environmental Engineering, Tianshui Normal University, Tianshui, 741001, China
[2]MOE Key Laboratory of Tibetan Plateau Land Surface Processes and Ecological Conservation / Qinghai Province Key Laboratory of Physical Geography and Environmental Processes, Xining, 810008, China
[3]Academy of Plateau Science and Sustainability, Xining, 810008, China

Correspondence to: Chengyong Wu (giswuchengyong@163.com)

Abstract. The Carnegie-Ames-Stanford Approach (CASA) model is widely used to estimate vegetation net primary productivity (NPP) at regional scales. However, the CASA is still driven by multi-source data, e.g., satellite remote sensing (RS) data, and ground observations that are time-consuming to obtain. RS data can conveniently provide real-time regional information and may replace ground observation data to drive CASA model. We attempted to improve the CASA model in this study using the Moderate Resolution Imaging Spectroradiometer RS products, the GlobeLand30 RS product, and the Digital Elevation Model data derived from radar RS. We applied it to simulate the NPP of alpine grasslands in Qinghai Lake Basin, which is located in the northeastern Qinghai-Tibetan Plateau, China. The accuracy of the RS data driven CASA, with mean absolute percent error (MAPE) of 22.14% and root mean square error (RMSE) of 26.36 g C•m^{-2}•month^{-1}, was higher than that of the multi-source data driven CASA, with MAPE of 44.80% and RMSE of 57.43 g C•m^{-2}•month^{-1}. The NPP simulated by RS data driven CASA in July 2020 shows an average value of 108.01±26.31 g C•m^{-2}•month^{-1}, which is similar to published results and comparable with the measured NPP. The results of this work indicate that simulating alpine grassland NPP with satellite RS data rather than ground observations is feasible. We may provide a workable reference for rapid simulating grassland NPP to satisfy the requirements of accounting carbon stocks and other applications.

1 Introduction

Net primary productivity (NPP) is defined as the net accumulation of organic matter through photosynthesis by green plants per unit of time and space (Yu et al., 2009). NPP reflects the carbon sink, production, and food supply capacity of an ecosystem (Jiao et al., 2018; Li et al., 2019), so it plays an important role in studying carbon cycles, ecosystem management, grassland productivity (Zhang et al., 2016), crop yields (Wang et al., 2019), climate change (Zhang et al., 2018), and other issues directly or indirectly at both local and global scales (Li et al., 2020a). NPP has been the subject of attention from academics and governmental agencies (Wang et al., 2017), which is recognized as a key indicator by the International Biological Program (IBP, Uchijima and Seino, 1985), the International Geosphere Biosphere Program (IGBP, Terrestrial

Carbon Working Group, 1998), the Global Change and Terrestrial Ecosystem (GCTE, Fang et al., 2003), and the Kyoto Protocol.

Direct field measurements are time-consuming and costly, so simulation models are generally used to analyse NPP (Hadian et al., 2019). Existing NPP simulation models can be roughly split into three categories: climate relative models, process models, and Light Use Efficiency (LUE) models. LUE models include the Carnegie-Ames-Stanford Approach (CASA) model (Potter et al., 1993; Field, et al., 1995), carbon fixation model (Veroustraete et al., 2002), carbon flux model (Turner et al., 2006), etc. Among them, the CASA is a process-based model that describes processes of carbon exchange between the terrestrial biosphere and atmosphere (Cramer et al., 1999); it has been widely used to simulate regional or continental NPP over hundreds of published studies (Jay et al., 2016).

The parameters of CASA model are total solar radiation (SOL), fraction of absorbed photosynthetically active radiation (FPAR), water stress coefficient (WSC), temperature stress factors $T_{\varepsilon 1}$ and $T_{\varepsilon 2}$, and the maximum possible efficiency (ε_{max}). At regional scales, the FPAR is usually calculated by remote sensing (RS) data (e.g., Potter et al., 1993; Pei et al., 2018), and the ε_{max} for vegetation types is usually determined by Land-use and land-cover change (LUCC). Wang et al. (2017) used MODIS LUCC product (MCD12Q1) in the CASA model to determine the ε_{max} for each vegetation type. $T_{\varepsilon 1}$ and $T_{\varepsilon 2}$ are usually calculated by the air temperature data from ground meteorological stations through spatial interpolation method. SOL, a basic driver of CASA model, is usually calculated via Angstrom-Prescott equation or simulated by a solar radiation flux (SolarFlux) model. The Angstrom-Prescott equation (Prescott, 1940) uses measured solar radiation data to determine empirical coefficients a (the ratio of surface solar radiation to astronomical radiation under completely cloudy conditions) and b (the transmission characteristics of clouds to solar radiation), then SOL can be calculated using sunshine duration data from ground meteorological station. The SolarFlux model simulates SOL using the key parameter of Digital Elevation Model (DEM) that derived from radar RS, whose simulation precision mainly depends on the accuracy of atmospheric conditions. When astronomical solar radiation passes through the atmosphere, it is weakened by atmospheric scattering and absorption, and finally transmits to earth surface (so-called surface solar radiation), which means atmospheric conditions significantly affect surface solar radiation. The total cloud cover can greatly affect the atmospheric conditions, so it is helpful that introducing total cloud cover to simulate SOL. However, the SolarFlux model introducing total cloud cover has rarely reported so far. The WSC, another basic driver of the CASA model, is traditionally obtained using a ratio of the actual/estimated evapotranspiration (ET) to the potential evapotranspiration (PET). Initially, both ET and PET are determined from a soil moisture (SM) submodel. This model needs meteorological temperature and precipitation data as well as soil texture, soil depth, and other soil parameters typically obtained from a soil database or field investigation. ET and PET can also be calculated separately with different simulation models and data sources. PET is often calculated by the FAO Penman-Monteith equation (Allen et al., 1998), which needs meteorological observation data as input parameters; ET can be obtained with models based on the complementary relationship of evapotranspiration (Bouchetr,1963) or other approaches such as the Pike equation (Pike,1964). As such parameters are numerous, difficult to obtain, and complex to calculate, scholars have improved WSC by modifying ET or PET (e.g., Xu and Wang, 2016; Zhang et al., 2016; Pei et al., 2018). A

few scholars attempted to introduce RS data for improving WSC, but their techniques still need the support of ground observation data. For examples, Bao et al. (2016) introduced RS data to establish a land-surface water index and ScaledP (the ratio between monthly precipitation amounts and the maximum monthly precipitation within the growing season for individual pixels of precipitation) to improve WSC; Liu et al. (2018) improved WSC by the way of combining RS data and measured SM data.

In summary, CASA model is still driven by multi-source data, e.g., RS data and ground observations data. The parameter SOL can be simulated with radar RS data while it should be introduced total cloud cover to improve simulation accuracy. The parameters $T_{\varepsilon 1}$, $T_{\varepsilon 2}$ and WSC are dependent on ground meteorological data, soil data and other ground observation points data. The spatial distributions of these ground observation points are usually scattered and far apart. In some regions, there may be scant or even no observation stations, which drives down the application of CASA model. Moreover, due to the CASA needing to input continuous raster data, it means that the data of discrete observation points must be converted into continuous raster data of study area, which inevitably takes errors, and in turn affects the accuracy of simulation NPP. In addition, soil field measurements are time-consuming, and the monthly meteorological data and measured solar radiation data from meteorological departments are often published at a time delay, which makes it impossible to estimate NPP in real time. These factors prevent CASA from satisfying the requirements for accounting carbon stocks or other applications. Unlike ground observation points data, however, satellite RS can rapidly obtain regional data. Advancements in satellite sensor technologies and RS algorithms have yielded many LUCC data products (e.g., CCI-LC, MCD12, and GlobeLand30) and quality-controlled RS products, which are available online. GlobeLand30, a global LUCC data product, is widely used by scientists and users around the world (Chen et al., 2017). Moderate Resolution Imaging Spectroradiometer (MODIS) satellite sensor records cloud cover and land surface information. Some MODIS products, e.g., land surface temperature (LST) product, were evaluated in several previous studies (Wan et al., 2002; Zou et al., 2015) and applied in terms of air temperature estimation and other fields (Fu et al., 2011; Qie et al., 2020). Therefore, to drive a CASA model with an entire set of RS data, we used the MODIS products, GlobeLand30 product, and DEM data to improve CASA model as follows: (1)SOL was driven by total cloud cover data from MOD08_M3 product and DEM data; (2) FPAR was driven by Normalized Difference Vegetation Index (NDVI) data from MOD13Q1 product; (3)$T_{\varepsilon 1}$ and $T_{\varepsilon 2}$ were driven by LST data from MOD11A2 product; (4)SWC was driven by shortwave infrared reflectance data from MOD09A1 product; (5)ε_{max} was determined by vegetation types from GlobeLand30 product. The improved CASA that is called RS data driven CASA in this paper, was compared with multi-source data driven CASA, and was tested with the measured NPP of alpine grassland in Qinghai Lake Basin, in the northeast of Qinghai-Tibetan Plateau (QTP), China.

2 Data sources

2.1 Study area

Qinghai Lake Basin is located in the north-eastern QTP (Fig. 1). Its topography varies greatly over an altitude range of 3193-5114 m. It has a cold climate with an average annual air temperature of 1.2 ℃ (1951-2007). Its main vegetation types are alpine grasslands and alpine meadows, which account for 85.31% of all vegetation types. Qinghai Lake Basin was taken here as a study area to test the proposed RS data driven CASA model under conditions of varied topography and relative single vegetation types.

2.2 Data sources

2.2.1 DEM

DEM data with 90 m spatial resolution was derived from the Shuttle Radar Topography Mission as provided by the Geospatial Data Cloud (http://www.gscloud.cn/). It was aggregated into 500 m spatial resolution on the ArcGIS 10 software platform, then used to calculate SOL.

2.2.2 Solar radiation measurements

There is only one provincial ground solar radiation observation station in the study area. Observation data for the station in 2020 were not yet published at the time of this study, so we obtained its monthly SOL data for 2005, 2010, and 2015 from China Meteorological Data Service Center (http://data.cma.cn/) to verify the SOL simulation.

2.2.3 Ground meteorological data

The meteorological data of twenty ground observation stations in the study area and surrounding areas were obtained from China Meteorological Data Service Center (http://data.cma.cn/) and Qinghai Climate Center, Qinghai Province, China. The set contains average monthly data for years 2005, 2010, 2015, and 2020, including temperature (mean, minimum, maximum), sunshine duration (only for 2020), sunshine percentage, precipitation, wind speed, and relative humidity and served to calculate traditional SOL, traditional WSC, and input parameters of the multi-source data driven CASA model.

2.2.4 LUCC data

GlobeLand30 product at 30 m resolution in 2020, was obtained from GLOBELAND30 (http://www.globallandcover.com/) to identify grassland types and then determine its ε_{max}.

2.2.5 RS data

MODIS is a key sensor aboard the Terra and Aqua satellites. Terra MODIS and Aqua MODIS are covering the entire earth's surface every one to two days. The Earth Science Data Systems Program generates 8-day, 16-day, monthly, and other time-scaled quality-controlled MODIS products. The products MOD11A2, MOD09A1, MOD13Q1, and MOD08M3 were obtained from the National Aeronautics and Space Administration (NASA, https://ladsweb.modaps.eosdis.nasa.gov/search/). MOD 13Q1, MOD 09A1, and MOD 11A2, with spatial resolution ranging from 250 m to 1000 m, were resampled to 500 m spatial resolution via bilinear interpolation method. MOD08M3 was used to count total cloud cover unnecessarily adjusting its spatial resolution. Two images of 16-day products (MOD13Q1) and four images of 8-day products (MOD11A2, MOD09A1) were averaged separately to calculate the monthly CASA parameters.

AMSR2 products, a surface SM data set, have been evaluated in several previous studies and compared quite well with both observational and model simulation data sets from a variety of global test sites (Owe et al., 2008).We obtained the daily LPRM_AMSR2_DS_A_SOILM3 data of AMSR2 products in July 2020 from the Goddard Distributed Active Archive Center (DAAC, https://disc.gsfc.nasa.gov/) and averaged them to evaluate our WSC simulation results.

2.2.6 Field observation data

The field observation NPP data were surveyed via quadrat method. Referencing the Technical Regulations for Survey and Collection Biomass of Forest Carbon Pools (SACINFO, 2021) and the technical specification for field observation of grassland ecosystem (Ministry of Ecology and Environment, PRC, 2021), three 1 m × 1 m quadrats were designed in the corner of square sample plots 25 m × 25 m in size. The average NPP values of these three quadrats was regarded as the NPP value of the sample plot. All vegetation above ground in the quadrat was cut with scissors and placed into self-sealing bags, then placed into an oven at 105°C, baked for 15 min, and dried at 65 ◦C until reaching a constant dry biomass value. The dry aboveground biomass (AGB) value was converted to NPP as follows (Zhang, 2016):

$$NPP = AGB \times C(1 + SR)\,, \tag{1}$$

where *C* is carbon content coefficient converting biomass to NPP. It does not exceed 40% for herbaceous plants in the Tree-River Headwaters Region, QTP (Sun et al., 2017), and was set to 37.13% here according to the average carbon content of herbaceous plants (Zheng et al., 2007). *SR* represents the ratio of above-ground biomass to below-ground biomass. Liu et al. (2020) reported that the average root-shoot ratio (the ratio of below-ground and above-ground biomass) of alpine grassland is 6.87, so *SR* was set to 1.00/6.87, namely *SR* equals 0.146 in this case.

From July 23 to July 27, 2020, we investigated a total of 30 quadrats and obtained ten samples of NPP data to validate the RS data driven CASA model (Table 4).

3 Methods

3.1 CASA model

The CASA model incorporates meteorology, environment, and soil factors to simulate the physiological process of vegetation absorbing photosynthetically available radiation and transforming it into organic carbon. The model is (Potter et al., 1993; Wang et al., 2017):

$$NPP(x,t) = 0.5 \times SOL(x,t) \times FPAR(x,t) \times T_{\varepsilon 1} \times T_{\varepsilon 2} \times WSC(x,t) \times \varepsilon_{max} , \quad (2)$$

where *NPP* is the net primary production (g C•m^{-2}•month^{-1}); 0.5 represents the proportion of the radiation which can absorbed by plants(0.4-0.7 um); *SOL*(x,t) is the total solar radiation incident on grid cell x in a given month (MJ•m^{-2}•month^{-1}); *FPAR*(x,t) is the fraction of absorbed photosynthetically active radiation on grid cell x in a month; $T_{\varepsilon 1}$ and $T_{\varepsilon 2}$ are the temperature stress factors, representing the effect of high and low temperature on light utilization efficiency, respectively; *WSC*(x,t) is the water stress coefficient on grid cell x in a month; and ε_{max} is the maximum possible efficiency (g C•MJ^{-1}) under ideal conditions (no-stress temperature, no-stress water).

3.2 Improving CASA parameters with RS data

The RS data utilized here to improve CASA parameters are listed in Table 1. We focused specifically on improving the parameters SOL and WSC.

3.2.1 Calculation SOL by introducing RS total cloud cover

SolarFlux models (Hetrick et al., 1993; Kumar et al., 1997; Fu and Rich, 2002), which input DEM parameters and compute solar radiation over large areas, have been implemented for commercially available GIS software such as ARC/INFO, ArcGIS, and Genasys. The solar radiation module of ArcGIS software takes into account the influence of atmospheric conditions, latitude, altitude, solar zenith angle and azimuth angle, terrain shade, slope, and aspect. The atmospheric conditions relevant to the present study were determined by the parameters diffuse_proportion and transmittivity. The diffuse_proportion is the fraction of global normal radiation flux that is diffused, which is expressed as a values from 0 to 1. Transmittivity, the fraction of radiation that passes through the atmosphere, ranges from 0 (no transmission) to 1 (all transmission) (ESRI, 2021).

There are distinct differences between diffuse_proportion and transmittivity in both clear and cloudy days (i.e., dependent on total cloud cover). The accurate determination of atmospheric conditions is the key to accurately estimating SOL. We introduced satellite total cloud cover to classify weather conditions, then determined the corresponding diffuse_proportion and transmittivity values. The total cloud cover data from the MOD08_M3 product, ranging from 0 (where the sky is completely clear) to 10,000 (where the sky is completely covered by clouds), was divided by 1,000 to create ten levels. For each level, the diffuse_proportion and transmittivity were determined according to a simple linear relationship (Table 2).

3.2.2 Improvement WSC using shortwave infrared reflectance

WSC reflects the effect of available water content on the solar radiation utilization efficiency of plants, ranging from 0.5 (extreme drought conditions) to 1.0 (extreme humidity). According to the relation that shortwave infrared reflectance is negatively correlated with surface water content, scholars have proposed many water content RS indices. Referring to the form and connotation of the shortwave infrared soil moisture index (SIMI) proposed by Yao et al. (2011), we rewrote the WSC formula as follows:

$$WSC = 0.5 + 0.5(1 - N_{SIMI}) , \quad (3)$$

$$N_{SIMI} = (SIMI - SIMI_{min})/(SIMI_{max} - SIMI_{min}) , \quad (4)$$

$$SIMI = 0.7071\sqrt{SWIR_1{}^2 + SWIR_2{}^2} , \quad (5)$$

where *WSC* is the water stress coefficient; N_{SIMI} represents the normalized SIMI (ranging from 0 to 1); $SIMI_{max}$ and $SIMI_{min}$ are the maximum and minimum value of *SIMI* values, respectively; $SWIR_1$ and $SWIR_2$ are the shortwave infrared reflectance, respectively.

4 Results

4.1 SOL

4.1.1 SOL simulated by Angstrom-Prescott equation

The SOL of ground stations were obtained using ground meteorological data and Angstrom-Prescott equation (Table 1). Natural Neighbour spatial interpolation approach was applied to convert the SOL of ground stations into grid SOL over study area (Fig. 2-A).

4.1.2 SOL simulated by improved approach

The DEM, diffuse_proportion, and transmittivity determined by MODIS total cloud cover were input into the Solar Radiation module of ArcGIS10 software, then the SOL in July of 2020 was simulated in Qinghai Lake Basin(Fig. 2-B). The simulated SOL ranging from 655.42 MJ•m^{-2}•month^{-1} to 878.03 MJ•m^{-2}•month^{-1} with an average value of 738.80 MJ•m^{-2}•month^{-1}.The surface of Qinghai Lake shows the lowest SOL of 695.50 MJ•m^{-2}•month^{-1}. On the whole, SOL gradually increases along Qinghai Lake from southeast to northwest and is basically consistent with the actual total solar radiation.

4.1.3 Comparison of two SOL simulation approaches

We analysed the accuracy of simulation SOL from Angstrom-Prescott equation and improved SOL approach with the measured SOL monthly data in 2005, 2010, and 2015 (at present, only the measured SOL data in these period could be

collected for the purposes of this study, Table 3). The root mean square error (RMSE) of Angstrom-Prescott equation and our improved approach respectively are 162.24 MJ•m^{-2}•month^{-1} and 95.38 MJ•m^{-2}•month^{-1}.Correspondingly, the mean absolute percent error (MAPE) of two approaches are 24.56% and17.78%, the July RSME are 274.34 MJ•m^{-2}•month^{-1} and 70.66 MJ•m^{-2}•month^{-1}, and the July MAPE are 39.53% and 9.25%, respectively. For simulating SOL, the improved approach significantly increased the accuracy in the study area.

4.2 WSC

4.2.1 Traditional WSC

The WSC of ground stations were obtained using ground meteorological data for July 2020 and approaches listed in Table 1. Natural Neighbour approach was used to convert the WSC of ground stations into grid WSC over study area (Fig. 3-A).

4.2.2 Improved WSC

Using shortwave infrared reflectance of band 6 and band 7 from MOD09A1, We applied formula (3)-(5) and obtained the WSC in July, 2020(Fig. 3-C).The WSC values were relatively high (>0.86) around Qinghai Lake and in river valleys as well as in the river source areas at higher altitudes, which indicates that these places have sufficient water supply. The desert ecosystem in the east of the Qinghai Lake showed the lowest WSC (0.54-0.68), which indicates that the ecosystem has insufficient water supply.

4.2.3 Comparison of two WSC simulation approaches

WSC, a measure of the availability of water to plants, essentially reflects the impact of environmental water content on plants. For grassland ecosystem, to a certain extent, surface SM can indirectly reflect environmental water content. As a general rule, a higher value of WSC indicates a higher environmental water content. The surface SM data set (LPRM_AMSR2_DS_A_SOILM3) was used to evaluate the WSC results simulated by different approaches.

The SM is high in north of Qinghai Lake (Region N), and it is the lowest in the desert ecosystem (Fig. 3-B).In region N, the traditional WSC shows low values, which indicates that environmental water content is low, and the desert ecosystem showed a lower values, but not the lowest. Hence, the traditional WSC results are inconsistent with surface SM; they cannot reflect the spatial distribution of environmental water content accurately. The sparse distribution of ground meteorological stations caused uncertainty in the interpolation results.

The improved WSC results compared well with the surface SM in above two regions. Their spatial distribution are approximately consistent with the actual water contents in study area, so it is feasible to estimate WSC using RS shortwave infrared reflectance.

4.3 NPP

4.3.1 Comparison of multi-source and RS data driven CASA

The measured NPP obtained in July of 2020 was used to verify the accuracy of multi-source and RS data driven CASA models (Table 4). For the NPP simulated by multi-source data driven CASA (Fig. 4-A), the relative error (RE) ranges from 20.20% to 68.43%, the MAPE is 44.80%, the absolute error (AE) ranges from -112.88 g C•m^{-2} •$month^{-1}$ to -16.01 g C•m^{-2}•$month^{-1}$, and the RMSE is 57.43 g C•m^{-2}•$month^{-1}$.For the NPP simulated by RS data driven CASA, the RE ranges from 2.49% to 47.80%, the MAPE is 22.14%, the AE ranges from -34.54 g C•m^{-2}•$month^{-1}$ to 46.90 g C•m^{-2}•$month^{-1}$, and the RMSE is 26.36 g C•m^{-2}•$month^{-1}$. The simulation results of RS data driven CASA are more in accordance with the measured NPP, RS data driven CASA significantly increased the accuracy of grassland NPP in the study area.

4.3.2 NPP spatial distribution

The values of NPP simulated by RS data driven CASA are lower in the northwest parts of the basin and east of Qinghai Lake than elsewhere in the study area (Fig. 4-B). The main vegetation in the northwest is Alpine Kobresia humilis meadow plants such as *Saussurea pumila* and *Saussurea alpina*, which have low vegetation productivity and NPP values ranging from 0.33 g C•m^{-2}•$month^{-1}$ to 87.52 g C•m^{-2}•$month^{-1}$. The main vegetation in the southwest coast of Qinghai Lake and the middle part of the basin is *Stipa purpurea Griseb* and *Carex infuscata Nees* alpine grasslands, which have higher vegetation productivity and NPP values greater than 87.52 g C•m^{-2}•$month^{-1}$. NPP appears to decrease from southeast to northwest, which is consistent with the distribution patterns of vegetation type.

5 Discussion and recommendations

5.1 SOL

Various approaches for simulation SOL consider the atmospheric effects on solar radiation from different perspectives. The Angstrom-Prescott equation uses the sunshine duration (or sunshine percentage) to quantify atmospheric effects on solar radiation. We use the parameters of diffuse_proportion and transmittivity determined by total cloud cover to quantify these effects. The total cloud cover determines the weather conditions and affects the atmospheric conditions. Total cloud cover information can be used to directly determine weather conditions and indirectly determine atmospheric conditions. In this study, weather conditions were classified into ten levels according to the satellite total cloud cover. The two important parameters of the SolarFlux model, diffuse_proportion and transmittivity, were determined for each level on the basis of a linear relationship. The atmospheric conditions could be further divided into 100 or more refined levels to determine the values of diffuse_proportion and transmittivity under different cloud cover conditions to improve the SOL simulation accuracy.

It is important to note that the SolarFlux model is designed only for local landscapes/regional scales, so it is generally acceptable to use one latitude value for the whole DEM. It is necessary to divide larger areas into zones of varying latitude as the latitudes exceed 1 degree (ESRI, 2021).

5.2 WSC

Environmental water content can regulate vegetation NPP by affecting the photosynthetic capacity of plants. WSC reflects the influence of environmental water content on vegetation NPP. Traditional WSC simulation approach apply a ratio of ET to PET to measure the availability of environmental water content. ET and PET can be obtained by different approaches and data sources, resulting in substantial differences in ET and PET even if the same data is used, thus creating differences in WSC. The WSC result of our improved approach is certain as long as the same RS data is input in formula (3)-(5). In addition, the proposed WSC approach has the RS retrieval mechanism of environmental water content. Soil and vegetation water contents are closely related to their shortwave infrared spectral reflectance; small changes in these contents can cause substantial changes in shortwave infrared spectral reflectance. Thus, the RS shortwave infrared band is sensitive to environmental water content and can be used to calculate WSC. Many satellite sensors have shortwave infrared bands, such as MODIS (1.628-1.652 μm, 2.105-2.155 μm), LandSat 8 (1.560-1.660 μm, 2.100-2.300 μm), Sentinel-2(1.565-1.655 μm, 2.100-2.280 μm), and HJ-1-A, B (1.550-1.750 μm). Scholars have developed many RS water content indexes such as SIMI, MSIWSI (Dong et al., 2015) and SWCI (Du et al., 2007). We modified the WSC using SIMI and the two shortwave infrared bands of MODIS in this study. The shortwave infrared bands of satellite sensors mentioned above, as well as the MSIWSI, SWCI, or other RS water content indices, can also be considered to calculate WSC.

5. 3 Rationality of NPP simulation results

We compared our simulated NPP with previously published results (Table 5). Our simulated grassland NPP in July of 2020 has an average value of 108.01 ±26.31 g $C•m^{-2}•month^{-1}$, which is similar to the most published results, but smaller than some of them. Qinghai Lake Basin is located on the QTP, which has a severely cold climate and short growing season. Vegetation is in its growth stage in July and its biomass reaches the highest values for the whole year before the end of August or the beginning of September, which means that grassland NPP also reaches the annual maximum value about a month later. The reported NPP encompasses the full year, so it is reasonable that July NPP simulation values would be lower than some previously reported NPP values.

The simulation NPP values of *Kobresia parva* and *Stipa purpurea* are larger and smaller, respectively, than the measured NPP values. *Kobresia parva* is distributed in high-altitude areas where herdsmen often utilize as summer pastures. Grazing cattle and sheep reduce the biomass of these areas resulting in lower measured NPP values. *Kobresia parva* is characterized by low and short (1-3 cm) vegetation with densely clumped stems and high coverage. Grazing livestock does not significantly affect its reflectance at red and near infrared bands. For grazed and ungrazed *Kobresia parva*, the NDVI calculated by the reflectance of red and near infrared bands are almost the same; the FPAR values calculated by NDVI are

also very similar, so the simulated NPP values are nearly identical as well. Due to the lower measured NPP value of *Kobresia parva* caused by grazing, the NPP simulation values of *Kobresia parva* appear to be relatively high. *Stipa purpurea*, distributing in low-altitude areas where herdsmen often use as winter pastures, is an ideal vegetation type to verify the NPP model as it is not consumed by cattle, sheep, or other livestock during the summer. *Stipa purpurea* has a thin stalk up to 45 cm high and its leaf curled into needles with strongly lignified epidermes and purple spikelets. These characteristics result in a lower reflectance at red and near infrared bands, which leads to lower NDVI and FPAR values. Thus, the simulated NPP values of *Stipa purpurea* are relatively low.

5. 4 Uncertainty

According to equation (1), the uncertainty of measured NPP originates from uncertainties in AGB, C, and SR. There is randomness in which three quadrats are selected from the four corners of square sample plot, resulting in uncertainty AGB collection. In our case, C and SR are adopted the values reported in the literatures rather than measured values, which inevitably caused errors.

The uncertainty of multi-source data driven CASA and its parameters is mainly caused by spatial interpolation methods. The WSC interpolation results from Spline and Kriging method have significantly different values and spatial patterns (Fig. 5). The sample 7 has the maximum errors of estimation NPP (Table 4). Its SOL simulated by traditional approach is 271.39 $MJ \bullet m^{-2} \bullet month^{-1}$, which is obtained by interpolating the SOL of observation stations. The average simulated and measured SOL of Gangcha observation station is 434.59 $MJ \bullet m^{-2} \bullet month^{-1}$ and 692.71 $MJ \bullet m^{-2} \bullet month^{-1}$ respectively (Table 3). The distance of this station from the sample 7 is about 43 km. Hence for sample 7, the errors of multi-source data driven CASA is mainly caused by the parameter SOL and the spatial interpolation method.

The uncertainty of RS data driven CASA mainly stem from RS product data quality and uncertainty propagation across parameters. RS product usually have corresponding data quality assurance describing the uncertainty of each pixel (e.g., the uncertainty of production MOD11A2; details regarding quality assurance can be found online at: https://icess.eri.ucsb.edu/modis/LstUsrGuide/usrguide_index.html).The combined uncertainty of simulation NPP is determined by the uncertainty propagation from parameters. In our case, the combined uncertainty of grassland NPP is 108.01 ± 26.31 g $C \bullet m^{-2} \bullet month^{-1}$.The uncertainty contribution of alpine meadow and other grassland types, as well as uncertainty propagation and quantification, will be carried out systematically in future work.

6. Conclusions

The traditional CASA model driven by multi-source data such as meteorology, soil, and RS has notable disadvantages. In this study, we attempted to drive a CASA entirely by RS data. We conducted a case study of alpine grasslands in Qinghai Lake Basin to find that it is feasible to calculate the CASA parameters SOL, WSC, $T_{\varepsilon 1}$, and $T_{\varepsilon 2}$ using RS data. The estimated NPP results were reliable. The main conclusions of this work can be summarized as follows.

• Cloud cover was used to quantify the atmospheric effects on solar radiation. It is only necessary to use DEM and RS total cloud cover data to simulate SOL. The improved SOL simulation approach has monthly RMSE and MAPE of 95.38 $MJ•m^{-2}•month^{-1}$ and 17.78%, respectively.

• According to the RS retrieval mechanism of environmental water content, shortwave infrared reflectance was used to modify the WSC. The improved WSC simulation approach simplified input parameters. Its results are more consistent with the actual environment water contents than that of the traditional WSC in the study area.

• The RS data driven CASA, without the support of ground observation data (e.g., soil or meteorology), yields simulations in closer accordance with measured NPP values. The RE ranges from 2.49% to 47.80%, the MAPE is 22.14%, the AE ranges from -34.54 g $C•m•month^{-1}$ to 46.90 g $C•m^{-2}•month^{-1}$, and the RMSE is 26.36 g $C•m^{-2}•month^{-1}$. The simulated NPP values of *Kobresia parva* in the grazing area and *Stipa purpurea* are higher than and lower than the respective real values. The combined uncertainty of grassland NPP is 108.01 ±26.31 g $C•m^{-2}•month^{-1}$. Uncertainty propagation and quantification will be the focus of our future work.

Code and data availability. The code and data are available at supplement.

Supplement. The supplement related to this article is available online at: https://doi.org/...../gmd.....-supplement.

Author contributions. CW, CE, KC, XY, and DH contributed to the manuscript writing. CW contributed to the code writing. LH, BL and RW contributed to data processing. CW, YS and FL contributed to field investigation. YS, CL and FL contributed to laboratory experiment.

Competing interests. The authors declare that they have no conflict of interest.

Acknowledgements. We gratefully acknowledge the Geospatial Data Cloud, China Meteorological Data Service Center, GLOBELAND30 and NASA for providing the data of DEM, SOL, LUCC, MODIS and AMSR2 products.

Financial support. This research has been supported by the Young PhD Fund of Colleges and Universities in Gansu Province, China(2022QB-143), the National Philosophy and Social Science Foundation of China (14XMZ072,18BJY200), the National Natural Science Foundation of China (41761017,41661023), the Project of the Qinghai Research Center of Qilian Mountain National Park(GY1908), the Fuxi Innovation Team Project of Tianshui Normal University(FX202006), the Scientific and Technological Program of Gansu Province, China (21JR1RE293), the Project of the State Key Laboratory of Frozen Soil Engineering(SKLFSE202014), and the Colleges and Universities Innovation Ability Improvement Project of Gansu Educational Committee (2019B-134).

Review statement.

References

Allen, R.G., Pereira, L.S., Raes, D., and Smith, M.: Crop evapotranspiration—guidelines for computing crop water requirements—FAO irrigation and drainage Paper 56, Food and Agriculture Organization of the United Nations: Rome, Italy, available at: http://www.fao.org/docrep/X0490E/x0490e00.htm(last access: 5 July 2021), 1998.

Bao, G., Bao, Y., Qin, Z., Xin, X., Bao, Y., Bayarsaikan, S., Zhou, Y., and Chuntai, B.: Modeling net primary productivity of terrestrial ecosystems in the semi-arid climate of the Mongolian Plateau using LSWI-based CASA ecosystem model, INT J APPL EARTH OBS., 46, 84–93, https://doi.org/10.1016/j.jag.2015.12.001, 2016.

Bouchet, R.J.: évapotranspiration réelle et potentielle signification climatique, International Association of Hydrological Sciences., 62, 134–142, 1963.

Cai, Y., Zheng, Y., Wang, Y., and Wu, R.: Analysis of terrestrial net primary productivity by improved CASA model in Three-River Headwaters Region, Journal of Nanjing University of Information Science and Technology (Natural Science Edition)., 5, 34–42, http://dx.doi.org/10.3969/j.issn.1674-7070.2013.01.004, 2013(in Chinese).

Chen, Z., Shao, Q., Liu, J., and Wang, J.: Analysis of net primary productivity of terrestrial vegetation on the Qinghai-Tibet Plateau, based on MODIS remote sensing data, Sci. China Earth Sci., 55, 1306–1312, https://doi.org/10.1007/s11430-012-4389-0, 2012.

Chen, J., Cao, X., Peng, S., and Ren, H.: Analysis and Applications of GlobeLand30: A Review, ISPRS Int. J. Geo-Inf., 6, 230, https://doi.org/10.3390/ijgi6080230, 2017.

Cramer, W., Kicklighter, D.W., Bondeau, A., Moore III, B., Churkina, G., Nemry, B., Ruimy, A., Schloss, A.L., and the Participants of the Potsdam NPP Model Intercomparison.: Comparing global models of terrestrial net primary productivity (NPP): overview and key results, Glob Chang Biol., 5(Supply1. 1), 1–15, https://doi.org/10.1046/j.1365-2486.1999.00009.x, 1999.

Dong, T., Meng, L., and Zhang W.: Analysis of the application of MODIS shortwave infrared water stress index in monitoring agricultural drought, Journal of Remote Sensing., 19, 319–327, http://dx.doi.org/10.11834/jrs.20153355, 2015(in Chinese).

Du, X., Wang, S., Zhou, Y., and Wei, H.: Construction and validation of a new model for unified surface water capacity based on MODIS data, Geomatics and Information Science of Wuhan University., 32, 205–207, http://dx.doi.org/10.3969/j.issn.1671-8860.2007.03.005, 2007(in Chinese).

ESRI.: Area Solar Radiation, available at: https://desktop.arcgis.com/en/arcmap/latest/tools/spatial-analyst-toolbox/area-solar-radiation.htm, last access: 13 July 2021.

Fang, J., Piao, S., Field, C., Pan, Y., Guo, Q., Zhou, L., Peng, C., and Tao, S.: Increasing net primary production in China from 1982 to 1999, Front Ecol Environ., 1, 293–297, https://doi.org/10.1890/1540-9295(2003)001[0294:INPPIC]2.0.CO;2, 2003.

Field, C.B, Randerson, J.T, and Malmström, C.M.: Global net primary production: Combining ecology and remote sensing, Remote Sens Environ., 51, 74–88, https://doi.org/10.1016/0034-4257(94)00066-V, 1995.

Fu, G., Shen, Z., Zhang, X., Shi, P., Zhang, Y., and Wu, J.: Estimating air temperature of an alpine meadow on the northern Tibetan Plateau using MODIS land surface temperature, Acta Ecol. Sin., 31, 8–13, https://doi.org/10.1016/j.chnaes.2010.11.002, 2011.

Fu, P. and Rich, P.M.: A geometric solar radiation model with applications in agriculture and forestry, Comput Electron Agr., 37, 25–35, https://doi.org/10.1016/s0168-1699(02)00115-1, 2002.

Guo, X., He, Y., Shen, Y., and Feng, D.: Analysis of the terrestrial NPP based on the MODIS in the source regions of Yangtze and Yellow rivers from 2000 to 2004, J Glaciol Geocryol., 28, 512–518, 2006(in Chinese).

Hadian, F., Jafari, R., Bashari, H., Mostafa, T., and Clarke, K.: Estimation of spatial and temporal changes in net primary production based on Carnegie Ames Stanford Approach (CASA) model in semi-arid rangelands of Semirom County, Iran, J. Arid Land., 11, 477–494, https://doi.org/10.1007/s40333-019-0060-3, 2019.

Hetrick, W.A., Rich, P.M, Barnes, F.J., and Weiss S.B.: GIS-based solar radiation flux models, American society for photogrammetry and temote sensing technical papers, GIS. Photogrammetry, and Modeling., 3, 132–143, available at: http://professorpaul.com/publications/hetrick_et_al_1993_asprs.pdf(last access: 19 July 2021), 1993.

IGBP Terrestrial Carbon Working Group.: CLIMATE: The terrestrial carbon cycle: implications for the Kyoto protocol, Science., 280, 1393–1394, https://doi.org/10.1126/science.280.5368.1393, 1998.

Jay, S., Potter, C., Crabtree, R., Genovese, V., Weiss, D.J., and Kraft, M.: Evaluation of modelled net primary production using MODIS and landsat satellite data fusion, Carbon Balance and Management., 11, 1–13, https://doi.org/10.1186/S13021-016-0049-6, 2016.

Jiao, W., Chen, Y., Li, W., Zhu, C., and Li, Z.: Estimation of net primary productivity and its driving factors in the Ili River Valley, China, J Arid Land., 10, 781–793, https://doi.org/10.1007/s40333-018-0022-1, 2018.

Kumar, L., Skidmore, A.K., and Knowles, E.: Modelling topographic variation in solar radiation in a GIS environment, Int. J. Geographical Information Science., 11, 475–497, https://doi.org/10.1080/136588197242266, 1997.

Li, C., Sun, H., Wu, X., and Han, H.: An approach for improving soil water content for modeling net primary production on the Qinghai-Tibetan Plateau using Biome-BGC model, CATENA., 184, 104253, https://doi.org/10.1016/j.catena.2019.104253, 2020b.

Li, J., Zou, C., Li, Q., Xu, X., Zhao, Y., Yang, W., Zhang, Z., and Liu, L.: Effects of urbanization on productivity of terrestrial ecological systems based on linear fitting: a case study in Jiangsu, eastern China, Sci. Rep., 9, 17140, https://doi.org/10.1038/s41598-019-53789-9, 2019.

Li, J., Zhou, K., and Chen, F.: Drought severity classification based on threshold level method and drought effects on NPP, heor. Appl. Climatol., 142, 675–686, https://doi.org/10.1007/s00704-020-03348-4, 2020a.

Liu, L., Hu, F., Yan, F., Lu, X., Li, X., and Liu, Z.: Above-and below-ground biomass carbon allocation pattern of different plant communities in the alpine grassland of China, Chinese J. Ecol., 39, 1409–1416, http://dx.doi.org/10.13292/j.1000-4890.202005.011, 2020 (in Chinese).

Liu, Y., Hu, Q., He, H., Li, R., Pan, X., and Huang, B.: Estimation of total surface solar radiation at different time scales in China, Climate Change Research., 17, 175–183, http://www.climatechange.cn/EN/10.12006/j.issn.1673-1719.2020.054, 2021 (in Chinese).

Liu, Z., Hu, M., Hu, Y., and Wang, G.: Estimation of net primary productivity of forests by modified CASA models and remotely sensed data, Int J Remote Sens., 39, 1092–1116, https://doi.org/10.1080/01431161.2017.1381352, 2018.

Ministry of Ecology and Environment, PRC.: Technical specification for investigation and assessment of national ecological Status: Field observation of grassland ecosystem, available at: https://www.mee.gov.cn/ywgz/fgbz/bz/bzwb/stzl/202106/W020210615510937790570.pdf, last modified: 12 May 2021(in Chinese).

Myneni, R.B. and Williams, D.L.: On the relationship between FAPAR and NDVI, Remote Sens Environ., 49, 200–211, https://doi.org/10.1016/0034-4257(94)90016-7, 1994.

Owe, M.F., Jeu, R.D, and Holme, T.: Multisensor historical climatology of satellite-derived global land surface moisture, J. Geophys. Res., 113, F01002, https://doi.org/10.1029/2007JF000769, 2008.

Pei, Y., Huang, J., Wang, L., Chi, H., and Zhao, Y.: An improved phenology-based CASA model for estimating net primary production of forest in central China based on Landsat images, Int J Remote Sens., 39, 7664–7692, https://doi.org/10.1080/01431161.2018.1478464, 2018.

Piao, S. and Fang, j.: Terrestrial net primary production and its spatio-temporal patterns in Qinghai-Xizang Plateau, China during 1982-1999, Journal of Natural Resources., 17, 373-380, 2002(in Chinese).

Piao, S., Fang, J. and Guo, Q.: Application of CASA model to the estimation of Chinese terrestrial net primary productivity, Chinese Journal of Plant Ecology., 25, 603–608, http://dx.doi.org/10.3321/j.issn:1005-264X.2001.05.015, 2001(in Chinese).

Piao, S., Fang, J., and He, J.: Variations in vegetation net primary production in the Qinghai-Xizang Plateau, China, from 1982 to 1999, Clim Change., 74, 253–267, https://doi.org/10.1007/s10584-005-6339-8, 2006.

Pike, J.G.: The estimation of annual run-off from meteorological data in a tropical climate, J. Hydrol., 2, 116–123, https://doi.org/10.1016/0022-1694(64)90022-8,1964.

Potter, C.S, Randerson, J.T, Field, C.B, Matson, P.A, Vitousek, P.M, Mooney, H.A, and Klooster, S.A.: Terrestrial ecosystem production: A process model based on global satellite and surface data, Global Biogeochem Cycles., 7, 811–841, https://doi.org/10.1029/93gb02725, 1993.

Prescott, J.: Evaporation from water surface in relation to solar radiation, Transactions of the Royal Society of Australia., 64, 114–125, 1940.

Qiao, K. and Guo, W.: Estimating net primary productivity of alpine grassland in Qinghai Lake Basin, Bulletin of Soil and Water Conservation., 36, 204–209, http://dx.doi.org/10.13961/j.cnki.stbctb.2016.06.035, 2016(in Chinese).

Qie, Y., Wang, N., Wu, Y., and Chen, A.: Variations in winter surface temperature of the Purog Kangri ice field, Qinghai–Tibetan Plateau, 2001-2018, using MODIS data, Remote Sens., 12, 1133, https://doi.org/10.3390/rs12071133, 2020.

Running, S.W., Thornton, P.E., Nemani, R., and Glassy, J.M.: Global terrestrial gross and net primary productivity from the earth observing system, In: Sala O.E., Jackson R.B., Mooney H.A., Howarth R.W. (eds) Methods in Ecosystem Science, Springer, New York, NY, available at: https://doi.org/10.1007/978-1-4612-1224-9_4(last access: 10 July 2021), 2000.

SACINFO.: Technical regulations for survey and collection biomass of forest carbon pools, available at: http://dbba.sacinfo.org.cn/stdDetail/002d12ec5dca5460e8ade379e8f74fb4b5c83e4f2c50d41913c518a8e9e39ac5, last access: 18 October 2021.

Sun, Q., Li, B., Zhou, C., Li, F., Zhang, Z., Ding, L., Zhang, T., and Xu, L.: A systematic review of research studies on the estimation of net primary productivity in the Three-River Headwater Region, China, J. Geogr. Sci., 27, 161–182, https://doi.org/10.1007/s11442-017-1370-z, 2017.

Sun, Q., Li, B., Zhang, T., Yuan, Y., Gao, X., Ge, J., Li, F., and Zhang, Z.: An improved Biome-BGC model for estimating net primary productivity of alpine meadow on the Qinghai-Tibet Plateau, Ecol Modell., 350, 55–68, https://doi.org/10.1016/j.ecolmodel.2017.01.025, 2017.

Turner, D.P., Ritts, W.D., Styles, J.M., Yang, Z., Cohen, W.B., Law, B.E., and Thornton, P.E.: A diagnostic carbon flux model to monitor the effects of disturbance and interannual variation in climate on regional NEP, Tellus., 58, 476–490, https://doi.org/10.1111/j.1600-0889.2006.00221.x, 2006.

Uchijima, Z. and Seino, H.: Agroclimatic evaluation of net primary productivity of natural vegetations, J. Agr. Met., 40, 343–352, https://doi.org/10.2480/agrmet.40.343, 1985.

Veroustraete, F., Sabbe, H., and Eerens, H.: Estimation of carbon mass fluxes over Europe using the C-Fix model and euroflux Data, Remote Sens Environ., 83, 376–399, https://doi.org/10.1016/S0034-4257(02)00043-3, 2002.

Wan, Z., Zhang, Y., Zhang, Q., and Li, Z.: Validation of the land-surface temperature products retrieved from Terra Moderate Resolution Imaging Spectroradiometer data, Remote Sens Environ., 83, 163–180, https://doi.org/10.1016/s0034-4257(02)00093-7, 2002.

Wang, J., Liu, J., Shao, Q., Liu, R., Fan, J., and Chen, Z.: Spatial–temporal patterns of net primary productivity for 1988 to 2004 based on GLOPEM-CEVSA model in the “Three-River Headwaters” region of Qinghai Province China, Chin. J. Plant Ecol., 33, 254–269, http://dx.doi.org/10.3773/j.issn.1005-264x.2009.02.003, 2009(in Chinese).

Wang, X., Tan, K., Chen, B., and Du, P.: Assessing the spatiotemporal variation and impact factors of net primary productivity in China, Sci. Rep., 7, 44415, https://doi.org/10.1038/srep44415, 2017.

Wang, Y., Xu, X., Huang, L., Yang, G., Fan, L., Wei, P., and Chen, G.: An improved CASA model for estimating winter wheat yield from remote sensing images, Remote Sens., 11, 1088, https://doi.org/10.3390/rs11091088, 2019.

Wo, X., Wu L., Zhang J., Zhang L., and Liu W.: Estimation of net primary production in the Three-River Headwater Region using CASA model, Journal of Arid Land Resources and Environment., 28, 45–50, http://dx.doi.org/10.13448/j.cnki.jalre.2014.09.001, 2014(in Chinese).

Xu, H. and Wang, X.: Effects of altered precipitation regimes on plant productivity in the arid region of northern China, Ecological Informatics., 31, 137–146, https://doi.org/10.1016/j.ecoinf.2015.12.003, 2016.

Yao, Y., Qin, Q., Zhao S., and Yuan, W.: Retrieval of soil moisture based on MODIS shortwave infrared spectral feature, Journal of Infrared and Millimeter Waves., 30, 9–14, 2011(in Chinese).

Yu, D., Shao, H., Shi, P., Zhu, W., and Pan, Y.: How does the conversion of land cover to urban use affect net primary productivity? A case study in Shenzhen city, China, Agric For Meteorol., 149, 2054–2060, https://doi.org/10.1016/j.agrformet.2009.07.012, 2009.

Yuan, Z., Wang, Y., Xu, J., and Wu, Z.: Effects of climatic factors on the net primary productivity in the source region of Yangtze River, China, Sci. Rep., 11, 1376, https://doi.org/10.1038/s41598-020-80494-9, 2021.

Zhang, M., Lal, R., Zhao, Y., Jiang, W., and Chen, Q.: Estimating net primary production of natural grassland and its spatio-temporal distribution in China, Sci. Total Environ., 553, 184–195, https://doi.org/10.1016/j.scitotenv.2016.02.106, 2016.

Zhang, R., Liang, T., Guo, J., Xie, H., Feng, Q., and Aimaiti, Y.: Grassland dynamics in response to climate change and human activities in Xinjiang from 2000 to 2014, Sci. Rep., 8, 2888, https://doi.org/10.1038/s41598-018-21089-3, 2018.

Zhang, T., Cao G., Cao, S., Chen, K., Shan Z., Zhang, J.: Spatial-temporal characteristics of the vegetation net primary production in the Qinghai Lake Basin from 2000 to 2012, Journal of Desert Research., 35, 1072–1080, 2015(in Chinese).

Zhang, Y., Hu, Q., and Zou, F.: Spatio-temporal changes of vegetation net primary productivity and its driving factors on the Qinghai-Tibetan Plateau from 2001 to 2017, Remote Sens., 13, 1566, https://doi.org/10.3390/rs13081566, 2021.

Zhang, Y., Qi, W., Zhou, C., Ding, M., Liu, L., Gao, J., Bai, W., Wang, Z., and Zheng, D.: Spatial and temporal variability in the net primary production of alpine grassland on the Tibetan Plateau since 1982, J. Geogr. Sci., 24, 269–287, https://doi.org/10.1007/s11442-014-1087-1, 2014.

Zheng, W., Bao W., Gu B., He X., and Leng L.: Carbon concentration and its characteristic in terrestrial higher plants, Chinese Journal of Ecology., 26, 307–313, http://dx.doi.org/10.3321/j.issn:1000-4890.2007.03.002, 2007(in Chinese).

Zou, D., Zhao, L., Wu, T., Wu, X., Pang, Q., Qiao, Y., and Wang, Z.: Assessing the applicability of MODIS land surface temperature products in continuous permafrost regions in the central Tibetan Plateau, J Glaciol Geocryol., 37, 308-317, http://www.bcdt.ac.cn/EN/10.7522/j.issn.1000-0240.2015.0034, 2015(in Chinese)

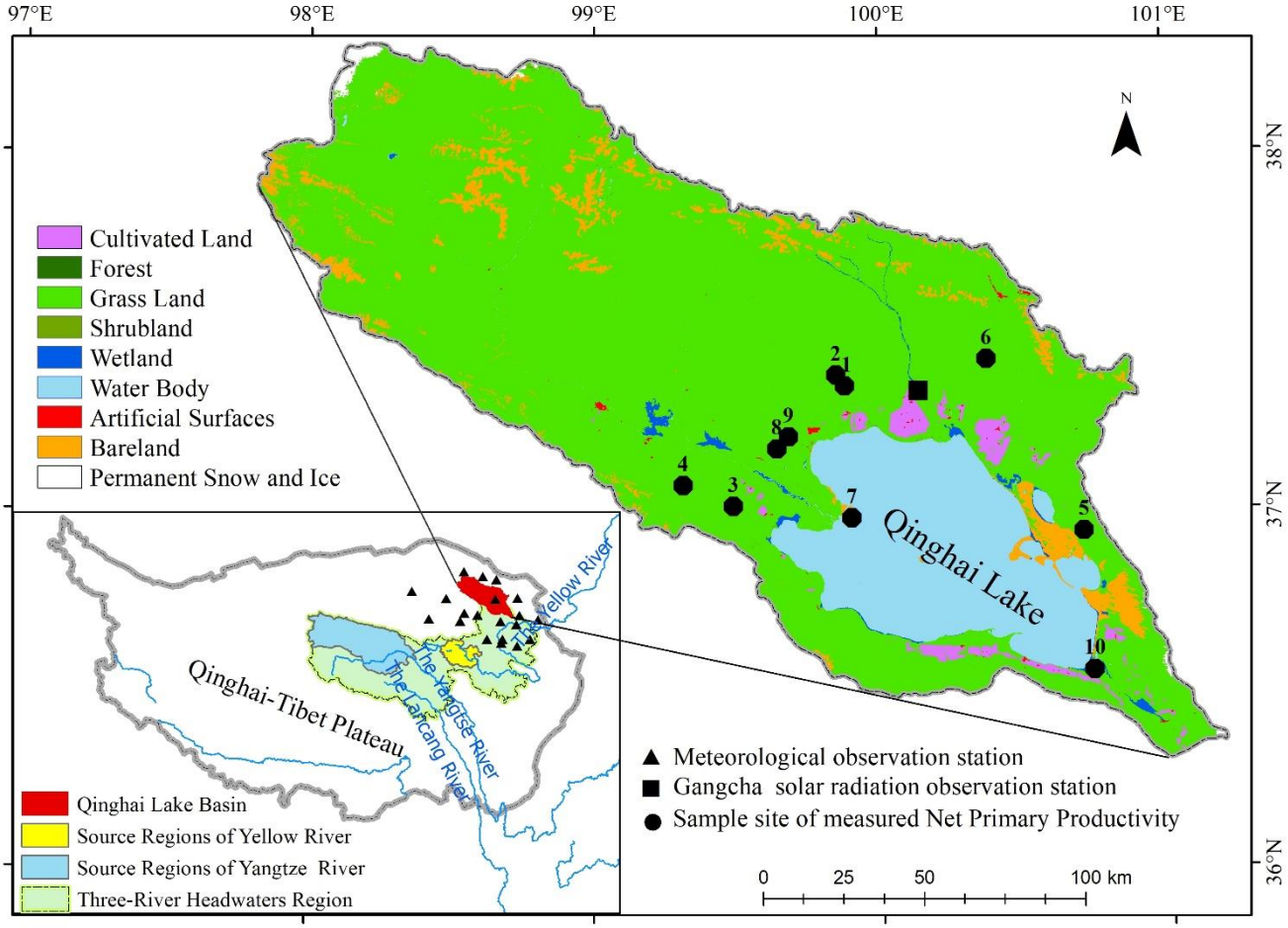

Figure 1. Location of Qinghai Lake Basin, sample and ground observation points.

Note: the land cover is the GlobeLand30 product in 2020, which was obtained from GLOBELAND30 (http://www.globallandcover.com/).

525

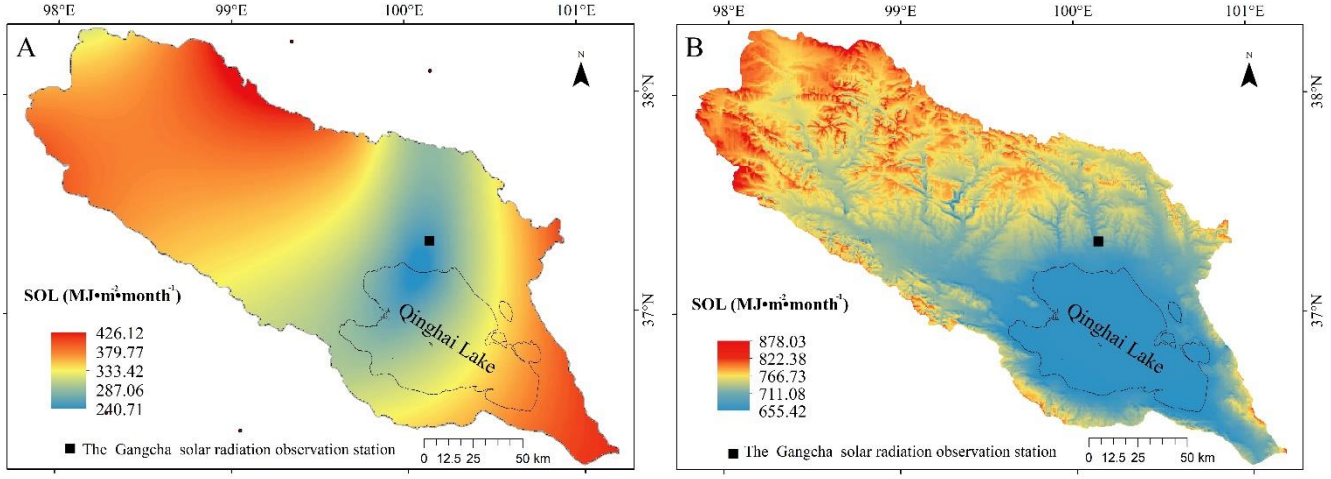

Figure 2. Spatial distribution of total solar radiation (SOL) in July, 2020. A, SOL simulated by Angstrom-Prescott equation. B, SOL simulated by improved approach.

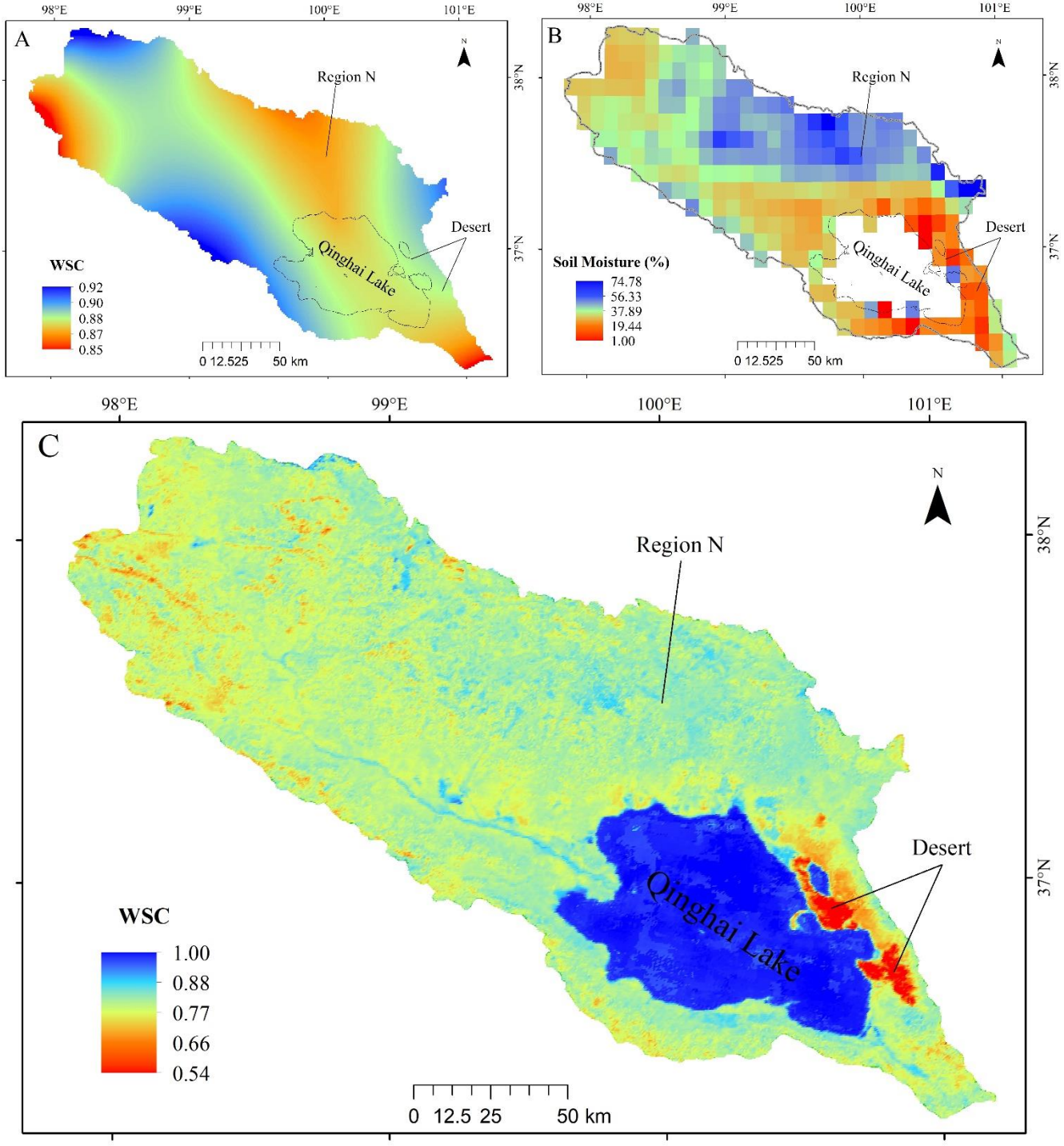

545

Figure 3. Spatial distribution of water stress coefficient (WSC) in July, 2020. A, WSC simulated by traditional method. B, Surface soil moisture of AMSR2 products. C, WSC calculated with RS shortwave infrared band.

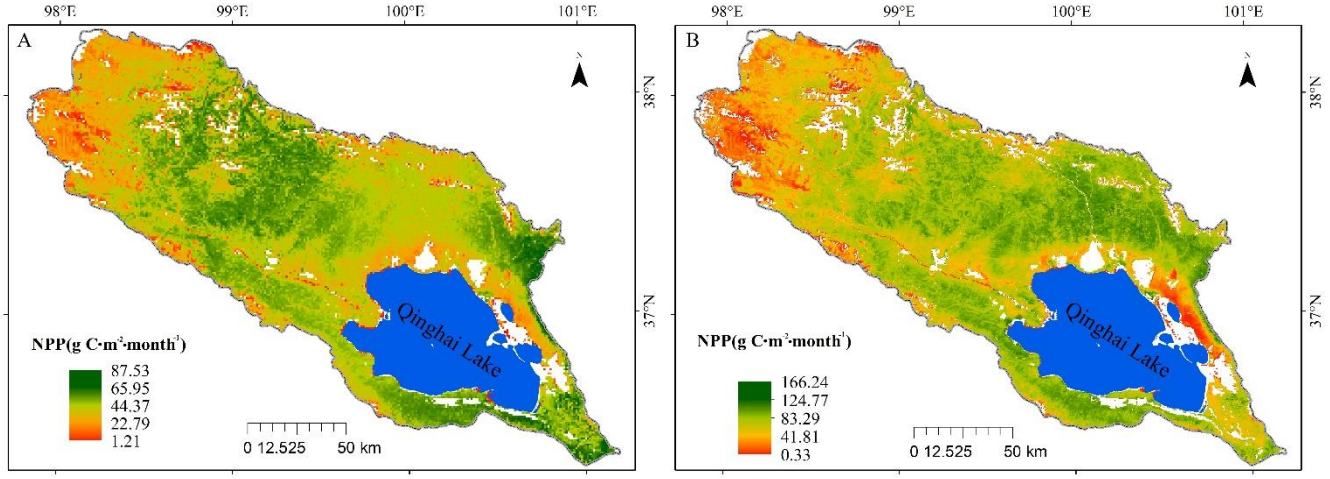

Figure 4. Spatial distribution of grassland net primary productivity (NPP) in July, 2020. A, NPP simulated by multi-source data driven CASA. B, NPP simulated by RS data driven CASA.

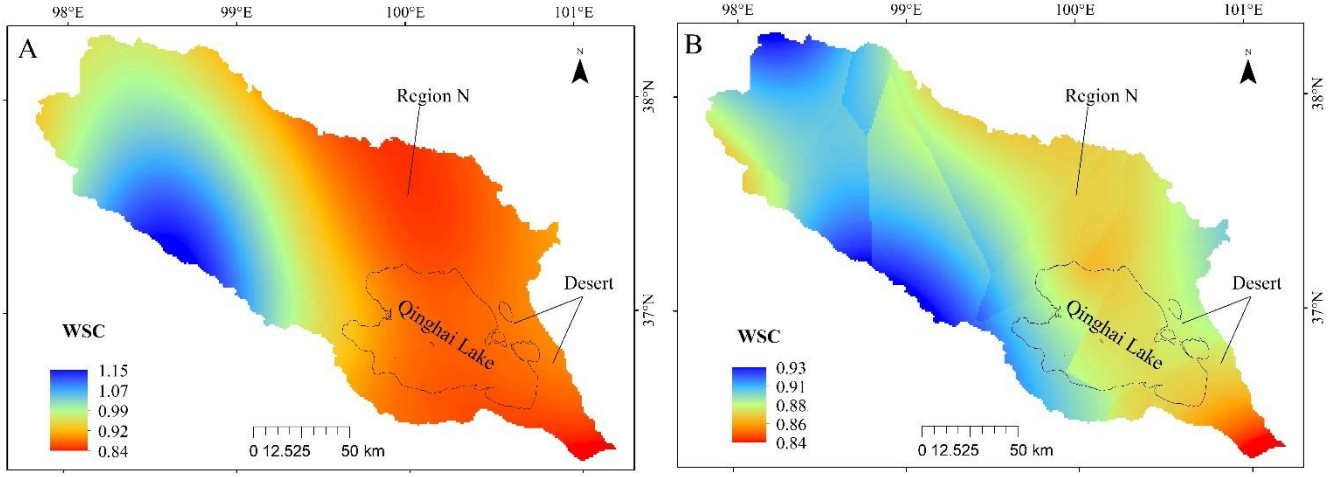

Figure 5. Comparison map of water stress coefficient (WSC) interpolation results in July, 2020. A, WSC from Spline method. B, WSC from Kriging method.

Table 1. Calculation method and input data for CASA model parameters

Parameter	RS data driven CASA	Multi-source data driven CASA
SOL	SolarFlux model. DEM data and MOD08M3 product.	Angstrom-Prescott equation (Prescott, 1940). The empirical coefficients a and b were adopted the monthly coefficients from Liu et al. (2021) and their July values are 0.24 and 0.46 respectively. Sunshine duration data from ground meteorological station.
WSC	Band 6 (1.628-1.652 μm) and band 7 (2.105-2.155 μm) from MOD09A1 product.	WSC=0.5+0.5(ET/PET), ET was calculated with Pike equation (Pike, 1964), and PET was calculated with FAO Penman-Monteith equation (Allen et al., 1998). Ground meteorological data.
$T_{\varepsilon1}$,$T_{\varepsilon2}$	$T_{\varepsilon1} = 0.8 + 0.02T_{0pt} - 0.0005(T_{opt})^2$ $T_{\varepsilon2} = 1.1814/\left[1 + e^{0.2(T_{opt}-10-T)}\right] \times \left[1/(1 + e^{0.3(-T_{opt}-10+T)})\right]$ (Potter et al., 1993). Temperature T=0.5(T_{day}+T_{night}), day temperature (T_{day}) and night temperature (T_{night}) from MOD11A2 product. The optimum temperature T_{opt} is the average value of T.	The equations of $T_{\varepsilon1}$ and $T_{\varepsilon2}$ are as same as that of RS data driven CASA. Monthly average temperature from ground meteorological data as T, and T_{opt} is the average value of T.
ε_{max}	ε_{max}=0.608g C•MJ^{-1}, maximum possible efficiency of grassland (Running et al., 2000).	The value of ε_{max} is as same as that of RS data driven CASA.
FPAR	$FPAR = \frac{(NDVI - NDVI_{min}) \times (FPAR_{max} - FPAR_{min})}{NDVI_{max} - NDVI_{min}} + FPAR_{min}$ *$NDVI_{min}$* and *$NDVI_{max}$* is the minimum and maximum of NDVI values from MOD13Q1 product. *$FPAR_{max}$* and *$FPAR_{min}$* are constants, with values of 0.95 and 0.001, respectively (Wang et al., 2017).	FPAR is the same as that of RS data driven CASA.

Table 2. Diffuse_proportion and transmittivity values under different total cloud cover levels

MODIS total cloud cover level	Weather conditions	Diffuse_proportion	Transmittivity
0	Very clear sky conditions (no clouds)	0.2	0.6
1	Cloud cover accounts for 1/9 of the whole sky	0.255	0.545
2	Cloud cover accounts for 2/9 of the whole sky	0.31	0.49
3	Cloud cover accounts for 3/9 of the whole sky	0.365	0.435
4	Cloud cover accounts for 4/9 of the whole sky	0.42	0.38
5	Cloud cover accounts for 5/9 of the whole sky	0.475	0.325
6	Cloud cover accounts for 6/9 of the whole sky	0.53	0.27
7	Cloud cover accounts for 7/9 of the whole sky	0.585	0.215
8	Cloud cover accounts for 8/9 of the whole sky	0.64	0.16
9	Sky is completely covered by clouds	0.695	0.105

Note: According to the scientific rule that diffuse_proportion has an inverse relation with transmittivity, the diffuse_proportion and transmittivity values were set to 0.2 and 0.6, respectively, in the case of a very clear sky conditions. Under other cloud cover conditions, their values were determined according to a simple linear relationship: $diffuse\_proportion = 0.2 + 0.055 level$, $transmittivity = 0.6 - 0.055 level$. The step length of 0.055 was determined by repeatedly testing.

Table 3. Measured versus simulated SOL

Date	Measured SOL ($MJ \cdot m^{-2} \cdot month^{-1}$)	Simulated SOL ($MJ \cdot m^{-2} \cdot month^{-1}$)	Absolute error (AE) ($MJ \cdot m^{-2} \cdot month^{-1}$)	Relative error (RE) (%)
Jan-05	374.19	240.95(477.62)	-133.24 (103.43)	35.61 (27.64)
Feb-05	427.29	319.23(469.44)	-108.06 (42.15)	25.29 (9.86)
Mar-05	573.16	489.16(528.34)	-84.00 (-44.82)	14.66 (7.82)
Apr-05	638.45	634.05(465.35)	-4.40(-173.10)	0.69 (27.11)
May-05	736.19	731.24(449.60)	-4.95 (-286.59)	0.67 (38.93)
Jun-05	663.70	742.68(394.28)	78.98 (-269.42)	11.90 (40.59)
Jul-05	626.92	710.94(385.94)	84.02 (-240.98)	13.40 (38.44)
Aug-05	603.86	623.86(423.19)	20.00 (-180.67)	3.31 (29.92)
Sep-05	493.09	500.53(407.90)	7.44 (-85.19)	1.51 (17.28)
Oct-05	486.07	378.72(521.19)	-107.35 (35.12)	22.09 (7.22)
Nov-05	398.73	257.36(481.56)	-141.37 (82.83)	35.46 (20.77)
Dec-05	353.71	197.43(456.82)	-156.28 (103.11)	44.18 (29.15)
SOL in 2005	6375.36	5826.15(5461.24)	-549.21 (-914.12)	8.61 (14.34)
Jan-10	354.87	262.42(484.86)	-92.45 (129.99)	26.05 (36.63)
Feb-10	409.77	295.56(457.35)	-114.21 (47.58)	27.87 (11.61)
Mar-10	555.98	456.14(509.99)	-99.84 (-45.99)	17.96(8.27)
Apr-10	647.71	634.05(496.56)	-13.66(-151.15)	2.11 (23.34)
May-10	705.07	731.24(449.60)	26.17 (-255.47)	3.71 (36.23)
Jun-10	616.64	649.32(368.04)	32.68 (-248.60)	5.30 (40.32)
Jul-10	741.78	756.37(436.54)	14.59(-305.24)	1.97 (41.15)
Aug-10	679.30	705.02(443.55)	25.72 (-235.75)	3.79 (34.71)
Sep-10	524.02	500.53(428.95)	-23.49 (-95.07)	4.48 (18.14)
Oct-10	496.53	378.72(499.47)	-117.81 (2.94)	23.73 (0.59)
Nov-10	450.87	299.47(507.51)	-151.40 (56.64)	33.58 (12.56)
Dec-10	371.24	181.71(446.67)	-189.53 (75.43)	51.05 (20.32)
SOL in 2010	6553.78	5850.55(5529.07)	-703.23 (-1024.71)	10.73 (15.64)
Jan-15	383.84	240.95(477.62)	-142.89 (93.78)	37.23 (24.43)
Feb-15	435.62	319.23(453.32)	-116.39 (17.70)	26.72 (4.06)
Mar-15	602.04	489.16(509.99)	-112.88(-92.05)	18.75 (15.29)
Apr-15	677.3	634.05(469.81)	-43.25 (-207.49)	6.39 (30.64)
May-15	664.51	731.24(408.32)	66.73(-256.19)	10.04 (38.55)
Jun-15	621.22	699.14(375.53)	77.92 (-245.69)	12.54 (39.55)
Jul-15	709.44	797.23(432.64)	87.79 (-276.80)	12.37 (39.02)
Aug-15	617.12	705.02(431.33)	87.90 (-185.79)	14.24 (30.11)
Sep-15	483.73	463.64(407.90)	-20.09 (-75.83)	4.15 (15.68)
Oct-15	509.48	432.73(538.56)	-76.75 (29.08)	15.06 (5.71)
Nov-15	370.52	257.36(459.33)	-113.16 (88.81)	30.54 (23.97)
Dec-15	338.99	197.43(456.82)	-141.56 (117.83)	41.76 (34.76)
SOL in 2015	6413.81	5967.18(5421.18)	-446.63(-992.63)	6.96 (15.48)
Jul-20	/	709.20	/	/

Note: The digits in parentheses "()" are the values of SOL simulated by Angstrom-Prescott equation and the corresponding error values.

Table 4. Measured versus simulated NPP

Samples	Main vegetation	Longitude	Latitude	Measured NPP (g C•m^{-2}•month^{-1})	Simulated NPP (g C•m^{-2}•month^{-1})	AE (g C•m^{-2}•month^{-1})	RE (%)
1	*Kobresia parva*	99.87586	37.34791	91.66	125.12 (56.58)	33.46 (-35.08)	36.50 (38.27)
2	*Kobresia parva*	99.84530	37.37877	98.12	145.02(62.68)	46.90 (-35.44)	47.80 (36.12)
4	*Kobresia parva*	99.30971	37.07243	110.54	116.92 (66.86)	6.38 (-43.68)	5.77 (39.52)
6	*Kobresia parva*	100.3727	37.42001	108.33	141.13 (65.67)	32.80 (-42.66)	30.28 (39.38)
9	*Stipa purpurea*	99.67833	37.20655	121.76	107.31 (53.08)	-14.45 (-68.68)	11.87 (56.41)
8	*Stipa purpurea*	99.63823	37.17360	126.86	117.57 (57.66)	-9.29 (-69.20)	7.32 (54.55)
3	*Carex pamirensis*	99.48503	37.01362	111.22	113.99 (55.08)	2.77 (-56.14)	2.49 (50.48)
10	*Achnatherum splendens*	100.73520	36.54971	79.25	99.27 (63.24)	20.02 (-16.01)	25.26 (20.20)
5	*Achnatherum splendens*	100.70610	36.93822	74.82	49.99 (41.41)	-24.83 (-33.41)	33.19 (44.65)
7	*Blysmus sinocompressus*	99.89820	36.97944	164.95	130.41 (52.07)	-34.54 (-112.88)	20.94 (68.43)
RMSE=26.36 g C•m^{-2}•month^{-1}, MAPE=22.14% (RMSE=57.43 g C•m^{-2}•month^{-1}, MAPE=44.80%)							

Note: The digits in parentheses "()" are the values of NPP simulated by multi-source data driven CASA and the corresponding error values.

625

Table 5. Published versus simulated NPP

Vegetation type	Study area	Study period	Mean NPP ($g\ C \bullet m^{-2} \bullet a^{-1}$)	Model/ product	Reporter
Grassland	Three-River Headwaters Region	1988–2004	160.90	GLOPEM-CEVSA	Wang et al., 2009
Grassland	Three-River Headwaters Region	2010	146.66	CASA	Wo et al., 2014
Grassland	QTP	2005–2008	135.00	GLO-PEM	Chen et al., 2012
Grassland	QTP	2001–2017	221.16	MODIS product (MOD17A3)	Zhang et al., 2021
Alpine grassland	Three-River Headwaters Region	2004–2008	129.41	CASA	Cai et al., 2013
Alpine grassland	QTP	1982–2009	120.80	CASA	Zhang et al., 2014
Alpine grassland	QTP	1982–1999	80.00	CASA	Piao and Fang, 2002
Alpine meadow	Three-River Headwaters Region	2004–2008	188.95	CASA	Cai et al., 2013
Alpine steppe	Source Regions of Yangtze and Yellow Rivers	2000–2004	79.34	MODIS product (MOD17A3)	Guo et al., 2006
Alpine steppe-meadow	China	2004–2005	109.03	CASA	Wang et al., 2017
Alpine meadows and tundra	China	1982–1999	137.00	CASA	Fang et al., 2003
Alpine meadows and tundra	China	1997	131.00	CASA	Piao et al.,, 2001
All vegetation	Source Region of Yangtze River	2000–2014	100.00	CASA	Yuan et al., 2021
All vegetation	QTP	2012–2014	175.10	Biome-BGC	Sun et al., 2017
All vegetation	QTP	2012	208.20	Biome-BGC	Li et al., 2020b
All vegetation	QTP	1982–1999	125.00	CASA	Piao et al., 2006
All vegetation	Qinghai Lake Basin	2000–2012	161.01	CASA	Zhang et al., 2015
All vegetation	Qinghai Lake Basin	2001–2011	168.03	CASA	Qiao and Guo, 2017